JOURNAL OF VIROLOGY, Oct. 2005, p. 12434–12446 Vol. 79, No. 19
0022-538X/05/$08.00+0 doi:10.1128/JVI.79.19.12434–12446.2005

Stem-Loop IV in the 5′ Untranslated Region Is a *cis*-Acting Element in Bovine Coronavirus Defective Interfering RNA Replication

Sharmila Raman[1] and David A. Brian[1,2]*

Departments of Microbiology[1] and Pathobiology,[2] University of Tennessee College of Veterinary Medicine, Knoxville, Tennessee 37996-0845

Received 4 March 2005/Accepted 24 June 2005

The 210-nucleotide (nt) 5′ untranslated region (UTR) in the positive-strand bovine coronavirus (BCoV) genome is predicted to contain four higher-order structures identified as stem-loops I to IV, which may function as *cis*-acting elements in genomic RNA replication. Here, we describe evidence that stem-loop IV, a bulged stem-loop mapping at nt 186 through 215, (i) is phylogenetically conserved among group 2 coronaviruses and may have a homolog in groups 1 and 3, (ii) exists as a higher-order structure on the basis of enzyme probing, (iii) is required as a higher-order element for replication of a BCoV defective interfering (DI) RNA in the positive but not the negative strand, and (iv) as a higher-order structure in wild-type (wt) and mutant molecules that replicate, specifically binds six cellular proteins in the molecular mass range of 25 to 58 kDa as determined by electrophoretic mobility shift and UV cross-linking assays; binding to viral proteins was not detected. Interestingly, the predicted stem-loop IV homolog in the severe acute respiratory syndrome (SARS) coronavirus appears to be group 1-like in that it is in part duplicated with a group 1-like conserved loop sequence and is not group 2-like, as would be expected by the SARS coronavirus group 2-like 3′ UTR structure. These results together indicate that stem-loop IV in the BCoV 5′ UTR is a *cis*-acting element for DI RNA replication and that it might function through interactions with cellular proteins. It is postulated that stem-loop IV functions similarly in the virus genome.

Higher-order RNA structural elements in the 5′ untranslated regions (UTR) of positive-strand RNA virus genomes are known in many cases to function as *cis*-acting elements in genome replication. Their mechanistic role may be that of serving a *cis*-acting function for translation (5, 6, 10, 12, 16, 27, 29, 38), for genome targeting to a replication complex (9), or for synthesis of the negative-strand antigenome (4, 11, 13, 17, 25, 29, 34, 37) or the positive-strand genome (2, 3, 11, 21, 25, 27, 38). They, furthermore, may function through interactions with viral (2–4, 11–14, 17) or cellular (3, 6, 12, 14, 17, 27, 34, 38) proteins, or with other genomic RNA elements (10, 16, 20, 21, 41), some of which may cause genome circularization, a postulated prerequisite for genome replication in some positive-strand RNA viruses (4, 10, 11, 16, 17, 20, 29, 41). We postulate that the conserved higher-order RNA structures in the coronavirus 5′ UTR function in *cis* for genome replication, and we have begun to test this hypothesis in the context of a helper virus-dependent bovine coronavirus (BCoV) defective interfering (DI) RNA replicon whose 5′ UTR is identical to that in the viral genome (7, 28).

Within the 210-nucleotide (nt) 5′ UTR of the BCoV genome (Fig. 1A), three RNA stem-loops, named stem-loops I to III, have been described that map within the 5′-terminal 116 nt (7, 28). Stem-loops I and II map between nt 1 and 84, a sequence required for DI RNA replication (7), but appear not to have precise higher-order counterparts in other coronavirus genomes. A poorly conserved stem-loop II homolog is predicted in other coronaviruses and in arteriviruses that harbors the leader-associated core signal for subgenomic mRNA synthesis, a heptamer in coronaviruses and a hexamer in arteriviruses (7, 36). Stem-loop III, on the other hand, shows phylogenetic conservation among group 2 coronaviruses, appears to have a homolog in coronavirus groups 1 and 3, including its property as a mapping site for the start codon of an intra-5′ UTR short open reading frame, and demonstrates, as a higher-order structure, a *cis*-acting function in BCoV DI RNA replication (28). Experimental evidence, furthermore, has indicated that the binding of both viral and cellular proteins may play a role in the function of stem-loop III (unpublished data).

Here, we have described a fourth predicted stem-loop, stem-loop IV, that maps at nt 186 to 215 and therefore lies mostly within the 210-nt BCoV 5′ UTR. We have (i) described its structural conservation with an apparent homolog in other group 2 coronaviruses, (ii) examined its higher-order structure by RNase mapping, (iii) tested its function in DI RNA replication through mutation analyses, and (iv) tested, by electrophoretic mobility shift and UV cross-linking assays, its role as a target for the binding of viral and cellular proteins. In addition, we have speculated on possible stem-loop IV homologs in coronavirus groups 1 and 3 and in the severe acute respiratory syndrome (SARS) coronavirus.

MATERIALS AND METHODS

Virus and cells. A DI RNA-free stock of the Mebus strain of BCoV at 4.5×10^8 PFU/ml was grown on the human rectal tumor cell line HRT-18 and used as a helper virus as previously described (28).

Plasmid constructs. Construction of pGEM3Zf(-) (Promega)-based pDrep 1 has been previously described (7). To construct the plasmid derivatives of pDrep 1 from which T7 RNA polymerase-generated DI RNA transcripts with stem-loop IV mutations were obtained for replication assays (summarized in Table 1), overlap PCR mutagenesis (28) was done using the oligonucleotides listed in Table 2. The strategy for constructing mutant derivatives pSLIV-mutL, pSLIV-

* Corresponding author. Mailing address: Department of Microbiology, University of Tennessee, Knoxville, TN 37996-0845. Phone: (865) 974-4030. Fax: (865) 974-4007. E-mail: dbrian@utk.edu.

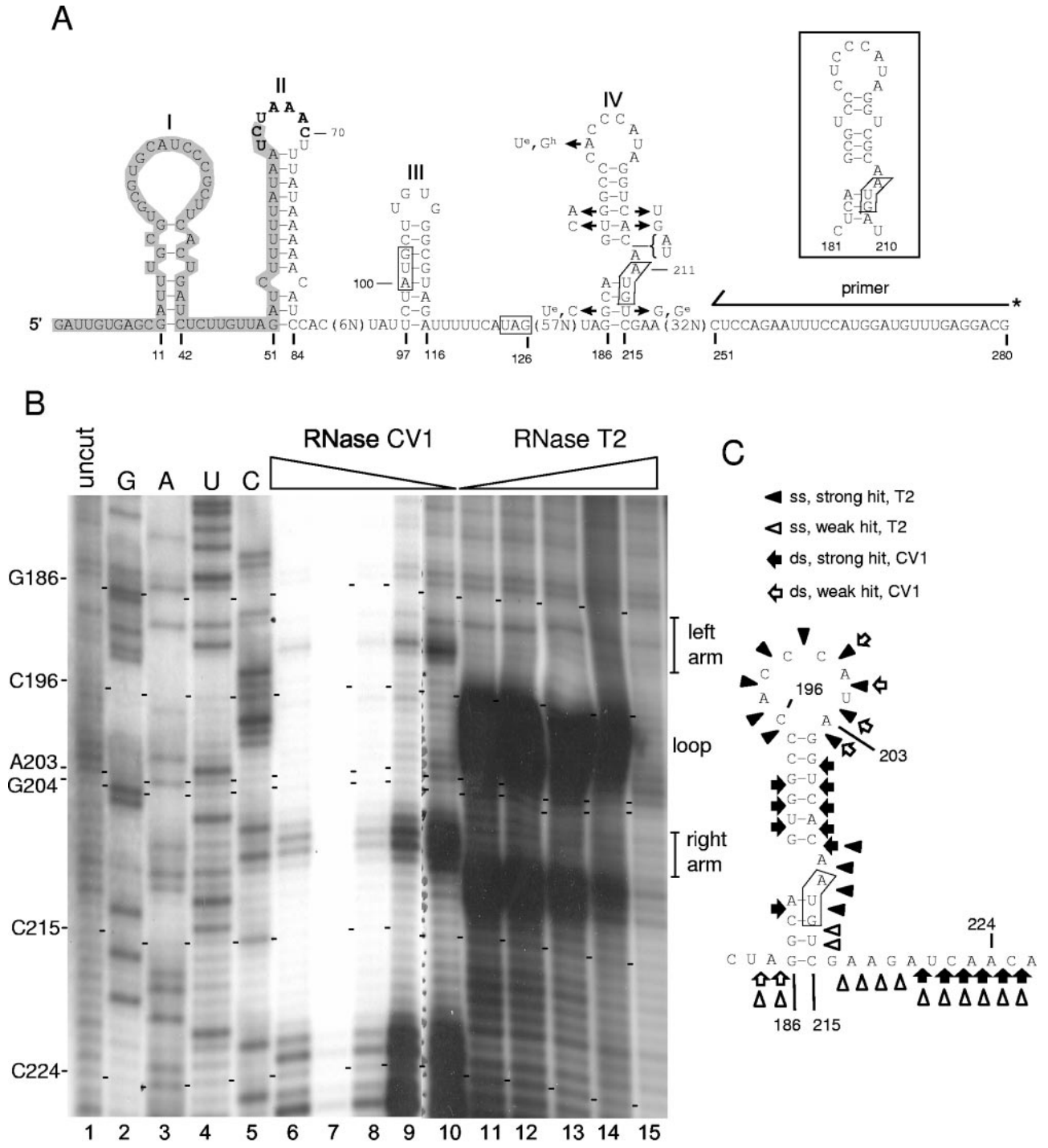

FIG. 1. Phylogenetic and enzyme structure probing evidence for stem-loop IV in BCoV genomic RNA. (A) Predicted secondary structures within the 210-nt 5′ UTR of the BCoV genome and the site from which the 5′-end-labeled primer was extended for stem-loop IV structure determination. The 65-nt BCoV leader sequence is shaded, and the leader-associated UCUAAAC intergenic sequence (nt 64 to 70, identified in bold) is found within loop II. The start and stop codons for the stem-loop III-associated intra-5′ UTR ORF and the start codon for ORF 1a are boxed. Previously described stem-loops I, II, and III are identified. Stem-loop IV is shown along with the variant bases found among the eight sequenced members of group 2 coronaviruses (see text). Bases with no superscript are found in all MHV strains (A59, 2, and JHM). Superscript identity: e, equine coronavirus; h, HCoV-OC43. Stem-loop IV is identical in BCoV, HEV, and HECoV. The predicted stem-loop IV homolog for the newly discovered HCoV-HKU1 is depicted in the inset. (B) Enzyme probing data for stem-loop IV. Depicted is a DNA sequencing gel showing separation of primer extension products. RNase digestion conditions for the double-strand-digesting RNase CV1 and single-strand-digesting RNase T_2 are described in the text. Lanes 2 to 5 show the products of an RNA sequencing reaction done on undigested RNA to identify the base positions. (C) Summary of enzyme probing data shown in panel B.

TABLE 1. Summary of stem-loop IV mutations

Mutant name[a]	Sequence in stem-loop IV mutant (nt 186 to 215)	Property of stem-loop IV mutant	Free energy (kcal/mol)		Binds cell proteins of:		Replication[c]
			+ strand[b]	− strand[b]	25, 26, 28, 39, 41 and 58 kDa	33, 45 and 48 kDa	
pDrep1 (wt)	–GGCAGUGGCCCACCCAUAGGUCACAAUGUC–	wt	−9.8	−6.7	Yes	Yes	Yes
pSLIV-mutdel	–ΔΔΔΔΔΔΔΔΔΔΔΔΔΔΔΔΔUCACAAUGUC–	Stem-loop mostly removed	No struct..	No struct.	No	Yes	No
pSLIV-mutL	–GGCAGacuggCACCCAUAGGUCACAAUGUC–	Stem is disrupted	No struct.	No struct.	No	Yes	No
pSLIV-mutR	–GGCAGUGGCCCACCCAUAccgguCAAUGUC–	Stem is disrupted	No struct.	No struct.	No	Yes	No
pSLIV-mutL/R	–GGCAGacuggCACCCAUAccgguCAAUGUC–	Stem is reformed	−9.8	−6.7	Yes	Yes	Yes
pSLIV-mutCA	–GGCAGcaGCCCACCCAUAGGUCACAAUGUC–	Stem-loop retained in (−); destabilized in (+) strand	−1.0	−5.1	No	Yes	No
pSLIV-mutGU	–GGCAGUGGCCCACCCAUAGGUugCAAUGUC–	Stem-loop retained in (+), destabilized in (−) strand	−6.7	−1.2	Yes	Yes	Yes
pSLIV-mutC198del	–GGCAGUGGCCCAΔCCAUAGGUCACAAUGUC–	C3 in loop is deleted	−9.8	−6.7	Yes	Yes	Yes
pSLIV-mut7	–GGCAGUGGCCCACuuAUAGGUCACAAUGUC–	C4 and C5 in loop are changed to Us.	−9.8	−6.7	No	Yes	No

[a] The wt and mutants listed were used for generating transcripts for structure studies (pDrep1) or replication assays (all). wt and mutants used for generating short transcripts for protein binding assays were, named, respectively, pSLIV-wt(PB), pSLIV-mutdel(PB), pSLIV-mutL/R(PB), pSLIV-mutR(PB), pSL-mutCA(PB), pSLIV-mutGU(PB), pSLIV-mutC198del(PB), and pSLIV-mut7(PB). Δ, deleted nucleotide; lowercase letters, changed nucleotides.

[b] In some cases, no structure was predicted by the Zuker algorithm, and this is indicated (no struct.).

[c] Said to be replicating if there was accumulation of DI RNA at 24 and 48 h posttransfection and the mutant form was present in cells infected with VP1.

mutGU, pSLIV-mutCA, pSLIV-mutC198del, and pSLIV-mut7 was the same as that for constructing pSLIV-mutR except that the appropriate corresponding primers described in Table 2 were used. For making pSLIV-mutR, primers SR673(+), mutR(-), and pDrep1 DNA were used in the first PCR, primers mutR(+), Forward(-), and pDrep1 DNA were used in the second reaction, and primers Forward(-) and SR673(+) and the products of the first two reactions were used in the third reaction to make a 710-nt product from which a 442-nt fragment was obtained with restriction endonucleases HpaI and XbaI and cloned into HpaI/XbaI-linearized pDrep1. For making pSLIV-mutL/R, pSLIV-mutL DNA replaced pDrep1 DNA in the first and second reactions. pSLIV-mutDel was made in two steps: (i) pSM3del was made by digesting pSM3 (pDrep1 with a G inserted at position 208) to create a SalI restriction enzyme site (8) with AvrII (at nt 183) and SalI (at nt 205), filling in with Klenow, and ligating; and (ii) G208 was removed from pSM3del by PCR mutagenesis using the corresponding primers and the procedure described for synthesis of pSLIV-mutR.

For making pSLIV(PB), identical to pDrep1 except that nt 4 through 152 are missing, thus enabling synthesis of 113-nt stem-loop IV-containing probes for testing protein binding, two steps were used. (i) An EcoRV restriction endonuclease site was created at nt 3 in pDrep1 by overlap PCR mutagenesis in which Nde1(+), SREcoR5(-), and pDrep1 DNA were used in the first reaction, SREcoR5(+), GEM3Zf(-)Nde1(-), and pDrep1 DNA were used in the second reaction, and GEM3Zf(-)Nde1(-), Nde1(+), and the products of the first two reactions were used in a third reaction to make a 1,183-nt product that was trimmed to 693 nt with restriction endonucleases NgoMIV and AvrII and cloned into NgoMIV/AvrII-linearized pDrep1. (ii) The resulting plasmid was digested with EcoRV and HpaI to remove nt 4 through 152, and the ends of the remaining fragment were ligated. The strategy used for making pSLIV-mutDel(PB) was the same as that for making pSLIV(PB) except that (i) pSLIV-mutDel DNA was used instead of pDrep1 DNA, (ii) the 1,163-nt product from the third PCR was trimmed to 663 nt with restriction endonucleases NgoMIV and HpaI, and (iii) the product was cloned into NgoMIV/HpaI-linearized pSLIV-mutDel DNA.

For making pSLIV-mutR(PB), pSLIV-mutL(PB), pSLIV-mutL/R(PB), pSLIV-mutC198del(PB), pSLIV-mut7(PB), pSLIV-mutGU(PB), and pSLIV-mutCA(PB), pSLIV(PB) was digested with NgoMIV and AvrII and the 545-nt fragment was cloned into the respective NgoMIV/AvrII-linearized mutant plasmids pSLIV-mutR, pSLIV-mutL, pSLIV-mutL/R, pSLIV-mutC198del, pSLIV-mut7, pSLIV-mutGU, and pSLIV-mutCA.

Enzyme structure probing of RNA. Enzyme structure probing was carried out essentially as previously described (28). Briefly, for in vitro synthesis of RNA, 10 μg of XbaI-linearized mung bean nuclease blunt-ended pDrep 1 DNA in a 200-μl reaction volume was transcribed at 37°C for 1 h with 80 U of T7 RNA polymerase (Promega) to yield approximately 40 μg of a 595-nt-long vector-free transcript. RNA was treated with 10 U of RNase-free DNase (Promega) at 37°C for 30 min, extracted with phenol-chloroform, chromatographed through a Bio-spin 6 column (Bio-Rad), spectrophotometrically quantified, and stored in water at −20°C. For RNase treatments, 40 μg of RNA was heat denatured at 65°C for 3 min and renatured by slow cooling (0.5 h) to 35°C in a 400-μl reaction volume containing 30 mM Tris HCl (pH 7.5)–20 mM $MgCl_2$–300 mM KCl, and aliquots containing 2 μg of sample RNA and 5 μg of yeast tRNA were incubated in 100 μl of the same buffer and 0.05, 0.5, 1, 2, or 4 U of RNase CV1 (Ambion), 0.05, 0.5, 1, 5, or 10 U of RNase T_1 (Gibco), or 0.05, 1, 2, 3, or 4 U of RNase T_2 (Gibco). RNase digestion was carried out at 25°C for 15 min and terminated by the addition of 150 μl of 0.5 M sodium acetate, after which the RNA was extracted with phenol-chloroform and ethanol precipitated. Digested RNA preparations were used in primer extension reactions with 5′-end-labeled plus-strand-binding oligonucleotide SR280(+) (Table 2; Fig. 1). Undigested RNA was used with the same primer in dideoxynucleotidyl sequencing reactions to generate a sequence marker. Products were analyzed on a DNA sequencing gel of 6% polyacrylamide.

Undigested RNA was used with the same primer in dideoxynucleotidyl sequencing reactions to generate a sequencing marker.

Northern assay for DI RNA replication. Northern assays were performed as previously described (7, 28). It should be noted that the synthetic oligonucleotide probe, TGEV8b(+), end labeled to specific activities of 1.5×10^5, is specific for the unique 30-nt reporter sequence in the DI RNA and therefore does not recognize native BCoV genomic or subgenomic mRNA sequences in the Northern assay.

Sequence analysis of the stem-loop IV region in progeny DI RNAs. For direct sequencing of asymmetrically amplified cDNA, the procedure of Hofmann et al. (18) for analysis of plus-strand RNA was used. Briefly, oligonucleotides TGEV8b(+) and SRleader(-) (Table 2) were used for reverse transcription-PCR with RNA extracted at 48 h postinfection (hpi) from cells infected with the first-passage virus (VP1) and in some cases second-passage virus (VP2), and

TABLE 2. Oligonucleotides used in this study

Oligonucleotide[a]	Polarity	Sequence (5′→3′)[b]	Binding region in pDrep1
Forward (−)	+	TAATACGACTCACTATA	3183–3200[c]
GEM3Zf(−)Ndel(−)	+	GAGAGTGCACCATATGCGGTGT	2498–2519[c]
Hpa1(+)	−	GGCTGAAAGCTGTTAACAGCAGAAATG	140–166
Hpa1(−)	+	CATTTCTGCTGTTAACAGCTTTCAGCC	140–166
mut7(−)	+	CCTAGGCAGTGGCCCACttATAGGTCACAATG	182–213
mut7(+)	−	CATTGTGACCTATaaGTGGGCCACTGCCTAGG	182–213
mutC198del(−)	+	CCTAGGCAGTGGCCCACCATAGGTCACAATG	182–213
mutC198del(+)	−	CATTGTGACCTATGGTGGGCCACTGCCTAGG	182–213
mutCA(−)	+	CGTGTTGTATCCTAGGCAGcaGCCCACCCATAGGTC	172–207
mutCA(+)	−	GACCTATGGGTGGGCtgCTGCCTAGGATACAACACG	172–207
mutG208del(−)	+	CGTGTTGTATCCTAGTCACAATGTCGAAGATC	172–222
mutG208del(+)	−	GATCTTCGACATTGTGACTAGGATACAACACG	172–222
mutGU(−)	+	GGCAGTGGCCCACCCATAGGTtgCAATGTCGAAGATCAACAAATACGGTC	186–235
mutGU(+)	−	GACCGTATTTGTTGATCTTCGACATTGcaACCTATGGGTGGGCCACTGCC	186–235
mutL(−)	+	GTATCCTAGGCAGactggCACCCATAGGTC	178–207
mutL(+)	−	GACCTATGGGTGccagtCTGCCTAGGATAC	178–207
mutL/R(−)	+	GactggCACCCATAccggtCAATGTCGAAGATC	190–222
mutL/R(+)	−	GATCTTCGACTTGaccggTATGGGTGccagtC	190–222
mutR(−)	+	GTGGCCCACCCATAccggtCAATGTCGAAGATC	190–222
mutR(+)	−	GATCTTCGACATTGaccggTATGGGTGGGCCAC	190–222
Ndel(+)	−	CCTCCAAATCATATGGACGTGTATTC	456–481
Nonly(+)	−	CCAGAACGATTTCCAAAGGACGCTCT	532–557
SR251(+)	−	CATCCATGGAAATTCTGGAG	251–270
SR280(+)	−	CGTCCTCAAACATCCATGGAAATTCTGGAG	251–280
SR5′UTR(−)	+	CATCCACTCCCTGTATTCTATGC	81–103
SR673(+)	−	CAAGAATAGTAGGGTACAAC	673–692
SRDM(+)	−	GTTGATCTTCGACATTGTGACC	204–225
SREcoR5(−)	+	GTGAATTGTAATACGACTCACTATAGATatcGAGCGATTTGCGTGCGTGC	3175[c]–25
SREcoR5(+)	−	GCACGCACGCAAATCGCTCgatATCTATAGTGAGTCGTATTACAATTCAC	3175[c]–25
SRleader(−)	+	GATTGTGAGCGATTTGCGTGCGTGC	1–25
TGEV8(+)	−	CATGGCACCATCCTTGGCAACCCAGA	1098–1123
TGEV8b(+)	−	CATGGCACCATCCTTGGCA	1105–1123

[a] The positive and negative symbols in the oligonucleotide names indicate the polarity of the nucleic acid to which the oligonucleotide anneals.
[b] Lowercase bases represent mutated sites.
[c] Indicates nucleotide positions in the circular pGEM3Zf(−) vector (Promega).

5′-end-radiolabeled oligonucleotide Hpa1(-), SRDM(+), SR251(+), or SR280(+) was used for sequencing.

Protein binding assays. Preparation of cell lysates essentially followed the procedure of Thomson et al. (35). Briefly, cells at 80% confluence in a 35-mm dish (~2×10^6 cells yielding lysate for about four gel-shift reactions) were mock infected or infected with BCoV (MOI = 10). AT 6 hpi, cells were washed with ice cold PBS, scraped into 500 μl cold PBS, pelleted at 600× *g* at 4°C for 4 min, resuspended in 400 μl lysis buffer (10 mM HEPES [pH 7.5], 3 mM $MgCl_2$, 14 mM KCl, 5% glycerol [vol/vol], 1.0% Nonidet P-40 [vol/vol], 1 mM dithiothreitol [DTT], 0.1 mM phenylmethylsulfonyl fluoride [PMSF]), incubated 20 min on ice, and then homogenized with 30 strokes in a tight-fitting Dounce homogenizer. The lysate was clarified at 700× *g* at 4°C for 10 min, the protein content, measured with a Bradford kit (Bio-Rad), was adjusted to 20 μg/10 μl with lysis buffer, and 10-μl aliquots were stored at −80°C.

For synthesis of uniformly radiolabeled RNA probe, plasmid DNA of wild-type (wt) pSLIV(PB) or the PB modifications of stem-loop IV mutants (Table 1) was linearized with NcoI, and 2.5 μg was transcribed in a 50-μl reaction volume with 40 U T7 RNA polymerase (Promega) at 37°C for 1 h in the presence of 120 μCi [α-^{32}P]UTP (300 Ci/mmole; ICN), 0.5 mM each of rATP, rCTP, and rGTP (Promega), 12 μM UTP (Promega), 10 mM DTT, and 5 mg acetylated bovine serum albumin (Promega). Radiolabeled RNA was treated with 2.5 U RNase-free DNase (Promega) at 37°C for 30 min, phenol-chloroform extracted, electrophoretically resolved on an 8 M urea–6% polyacrylamide gel after the addition of 50 μl loading dye (95% formamide, 20 mM EDTA, 0.3% bromophenol blue and xylene cyanol [wt/vol]). The resolved probe was visualized by X-ray film exposure to the wet gel, excised, and eluted by overnight agitation at 4°C in 2 ml of elution buffer (0.5 M ammonium acetate, 1 mM EDTA), extracted with phenol-chloroform, ethanol precipitated, dissolved in water to 2×10^4 cpm Cerenkov counts/μl, and stored at −80°C in 10-μl aliquots. Transcripts were 113 nt in length from all constructs except for those from pSLIV-mutdel(PB), which were 93 nt in length. Unlabeled transcripts used as competitor RNA were purified by chromatography through a Biospin 6 column (Bio-Rad).

For protein binding, essentially the conditions of Thomson (35) were used but with the addition of yeast tRNA (14) and heparin (6). Briefly, 10 μl of cell lysate (20 μg protein) was thawed and made 10 mM HEPES (pH 7.5), 3 mM $MgCl_2$, 14 mM KCl, 5% glycerol (vol/vol), 1.0% Nonidet P-40 (vol/vol), 1 mM DTT, 0.1 mM PMSF, 0.5 mg/ml yeast tRNA, and 0.05 mg/ml heparin by the addition of 10 μg of yeast tRNA and 1 μg heparin and from stocks, and the mixture was preincubated for 10 min at 30°C. Separately, 10 μl of RNA (2×10^4 cpm/μl) was thawed and mixed with 10 μl lysis buffer and preincubated for 30 min at 45°C. One microliter of the probe mixture (1×10^4 cpm) was then added to the 10 μl of preincubated protein lysate, and the total probe-protein mixture was incubated at 30°C for 10 min.

For electrophoretic separation of RNA-protein complexes, 2 μl of 50% glycerol was added to the probe-protein mixture and electrophoresis was carried out on a native gel of 6% polyacrylamide–5% glycerol at 4°C with 0.5× Tris-borate-EDTA (90 mM Tris HCl, 90 mM boric acid, 2 mM EDTA) for approximately 4 h at 100 V constant voltage.

For the electrophoretic mobility supershift assays, 2 μl of antiserum (containing approximately 40 μg of protein) was incubated with protein lysate either before or after the binding reaction with RNA probe as noted and the mixture was incubated an additional 30 min on ice (3, 13). Rabbit polyclonal anti-poly(C)-binding protein 2 (PCBP2) and preimmune sera (6) were kind gifts from E. Ehrenfeld (University of California, Irvine), and mouse polyclonal anti-La antiserum was obtained from BD Biosciences.

For UV cross-linking, the incubated probe-protein mixture was irradiated with 254-nm light on ice at 3 mW/cm^2 for 30 min in a Stratalinker (Stratagene). The mixture was then digested with 100 U RNase T_1 (Gibco), 2.5 U RNase A (Gibco), and 1 U RNase CV1 (Ambion) for 40 min at 37°C. For molecular weight determinations, radio-tagged proteins were resolved by sodium dodecyl

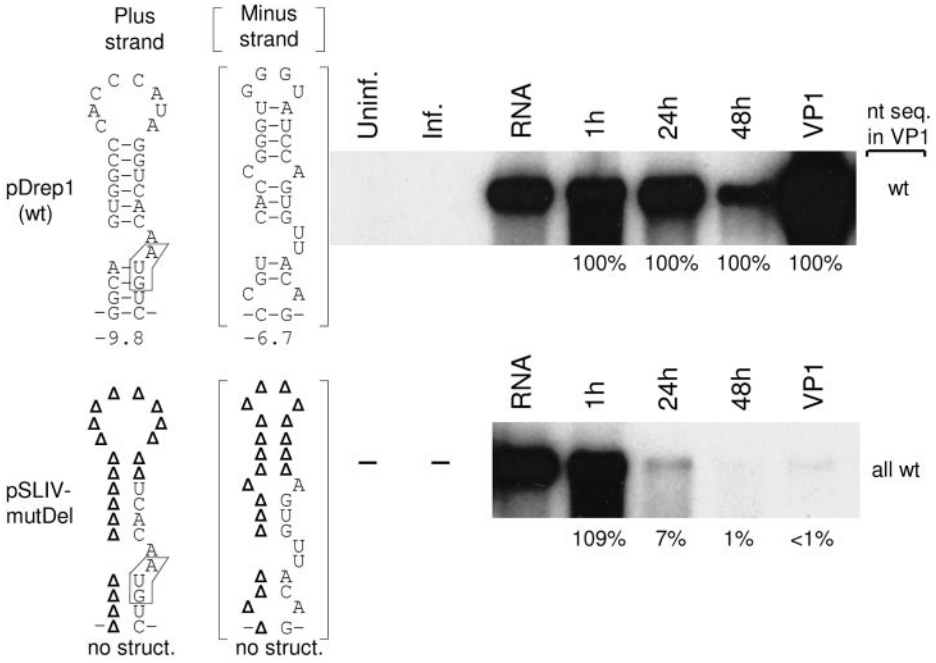

FIG. 2. Stem-loop IV-deleted DI RNA does not accumulate in helper virus-infected cells. The *mfold*-predicted structures of wt (pDrep1) and mutant (pSLIV-mutDel) transcripts in the positive and negative strands and their calculated free energies in kcal/mole are shown. Deleted bases in pSLIV-mutDel are represented by Δ. Accumulation was measured by Northern analysis with a reporter-specific radiolabeled oligonucleotide (see text). For Northern analyses, T7 RNA polymerase-generated transcripts of linearized plasmids were transfected into BCoV-infected cells and RNA was extracted at the indicated times posttransfection and at 48 h postinfection with VP1. Accumulation of pDrep1 progeny was considered to be 100%. The sequence of the RNA in VP1 progeny replicons was determined by bulk reverse transcription-PCR sequencing using pDrep1-specific primers as described in the text. Lanes: Uninf., mock-infected, nontransfected cells; Inf., infected, nontransfected cells; RNA, sample of the transcript.

sulfate-polyacrylamide gel electrophoresis (SDS-PAGE) in a gel of 10% polyacrylamide. Dried gels were exposed to Kodak XAB-S film 1 to 10 days for imaging.

All electrophoresis was done in gels of 140- by 0.75-mm dimensions.

Computer predictions of RNA secondary structures. The *mfold* algorithm of Zuker et al. (<http://www.bioinfo.rpi.edu/~zukerm/>) (24, 42) was used for secondary structure predictions. Predictions for all viruses described and for the wt and mutants of BCoV DI RNA were made in the context of a continuous genomic sequence of nt 1 to 500.

GenBank accession numbers of the sequences studied. GenBank accession numbers for the sequences studied are U00735 for BCoV-Mebus, AF523843 for HCoV-OC43, AF523844 for HECoV-4408, AF523845 for HEV-TN11, AF523846 for ECoV-NC99, AF201929 for MHV-2, NC001846 for MHV-A59, M55148 for MHV-JHM, NC006577 for HCoV-HKU1, NC002645 for HCoV-229E, NC005831 for HCoV-NL63, NC002306 for TGEV-Purdue 116, NC003436 for PEDV, NC001451 for IBV-Beaudette, and NC004718 for HCoV-SARS.

RESULTS

A predicted stem-loop IV in the BCoV 5′ UTR shows phylogenetic conservation among group 2 coronaviruses. Analysis of the 210-nt 5′ UTR and flanking sequence of the BCoV genome for RNA secondary structures with the *mfold* program of Zuker (24, 42) predicted a potential stem-loop with a stem of 10 bp containing a bulge of 2 nt, a terminal loop of 8 nt, and a free energy value of −9.8 kcal/mole (Fig. 1A). In the negative strand, a bulged stem-loop with a terminal tetraloop and a free energy of −6.7 kcal/mole was also predicted (Fig. 2).

The 5′ UTR sequences for 14 coronavirus species, including the SARS coronavirus, have been reported, enabling comparisons of predicted higher-order structures (see GenBank accession numbers given above). For the eight members in group 2 known at the beginning of this study, BCoV-Mebus, HCoV-OC43, HECoV-4408, HEV-67N, ECoV-NC99, MHV-2, MHV-A59, and MHV-JHM, high sequence conservation in the 5′ UTR had been noted (40) and the *mfold* program predicted a stem-loop IV homolog with small variations (stem-loop IV is identical among BCoV, HECoV, and HEV and is identical among MHV-2, MHV-A59, and MHV-JHM) (Fig. 1A). A newly reported group 2 coronavirus, human coronavirus HKU1 (39), also has a stem-loop IV homolog that varies only slightly from the other eight (Fig. 1A, inset). A possible homolog is also found in coronavirus groups 1 and 3 and in the SARS coronavirus (see Discussion). The predicted stem-loop IV for the eight group 2 coronaviruses examined in this study (i) has a stem of 10 bp with either a 2-nt bulge, as in BCoV, HCoV-OC43, HECoV, HEV, and ECoV, or a 4-nt bulge, as in MHV-2, MHV-A59, and MHV-JHM, with net negative free energies ranging from −12 to −9.8 kcal/mole, (ii) has an 8-nt terminal loop whose sequence is identical in BCoV, HECoV, HEV, MHV-2, MHV-A59, and MHV-JHM but differs at the second nucleotide position in HCoV-OC43 and ECoV, (iii) has a negative-strand counterpart with net negative free energies ranging from −8.9 to −6.7 kcal/mole, and (iv) begins at nt 183 for MHV-2 and MHV-A59, nt 185 for ECoV, nt 186 for BCoV, HCoV-OC43, HECoV, and HEV, and nt 188 for MHV-JHM. The predicted stem-loop IV for the newly reported HCoV-HKU1 conforms largely to that in HCoV-OC43 and ECoV except that it has a stem of 8 bp, an internal 2-nt

loop at nt 188, net negative free energies of −7.1 and −7.7 kcal/mole in the positive- and negative-strand forms, respectively, two covariant base differences in the stem, and begins at nt 181.

Thus, since a predicted stem-loop IV showed phylogenetic conservation in the eight group 2 coronaviruses examined at the beginning of this study, it was postulated to be a higher-order *cis*-acting element in BCoV DI RNA replication.

Enzyme structure probing supports the existence of stem-loop IV in BCoV RNA. An in vitro-synthesized 595-nt transcript of XbaI-linearized pDrep 1 DNA was digested with either double-strand-specific RNase CV1 or with single-strand-specific RNases T_1 (data not shown) or T_2, and the products were analyzed by reverse transcriptase extensions of the 5′-end-labeled primer SR280(+) (Fig. 1B, lanes 6 to 15). Radiolabeled products of an RNA sequencing reaction were analyzed in parallel to determine the sites of RNase digestion (Fig. 1B, lanes 2 to 5). Enzyme probing indicated that the upper part of the stem (nt 190 to 195 and 204 to 209) is susceptible to digestion by only RNase CV1 and is therefore probably stably base-paired, whereas the lower part of the stem (nt 186 to 189 and 212 to 215) appears susceptible to both RNases CV1 and T_2 and might represent a breathing structure in which a base-paired state alternates with a single-stranded region. The predicted loop of stem-loop IV, on the other hand, is strongly digested by RNase T_2 and is therefore likely to be a single-stranded region, consistent with it being a loop, as predicted. Weak hits with RNase CV1 at nt 200 to 204 suggest that these bases within the loop may at times pair with another region of the RNA. The results of enzyme structure probing overall show single- and double-stranded regions, in agreement with an *mfold*-predicted structure for stem-loop IV (Fig. 1C).

Integrity of stem IV is required for BCoV DI RNA replication. The rationale applied here for evaluating the functional importance of an RNA element in DI RNA replication has been previously described (28). Briefly, an element was deemed required if its removal or structural disruption by mutation led to a loss of DI RNA accumulation at 24 and 48 h posttransfection (hpt) and an absence of the mutated element in progeny molecules in VP1 RNA. In the case of a disrupted helical region, if restoration of the stem by compensatory mutations led to restored accumulation at 24 and 48 posttransfection and the presence of the double mutant in VP1 RNA, then this structure was judged to be a required *cis*-acting element for replication. In an initial test to examine the requirement of stem-loop IV in DI RNA replication, mutant pSLIV-mutDel was tested in which essentially the entire stem-loop was deleted (Table 1; Fig. 2). By Northern analysis, 7% and 1% of wt levels of DI RNA had accumulated by 24 and 48 hpt, respectively, and less than 1% had accumulated by 48 hpi in VP1. Sequence analysis of asymmetrically amplified cDNA from VP1 DI RNA, however, showed all progeny to be wild type as a result of copy choice recombination with the helper virus genome (8, 23) and hence revertants, indicating the deletion mutant had not replicated.

To examine the importance of the helical nature of stem IV in DI RNA replication, mutants pSLIV-mutL and pSLIV-mutR were made in which five of the six base pairs in the upper helix were disrupted in the left and right arms, respectively,

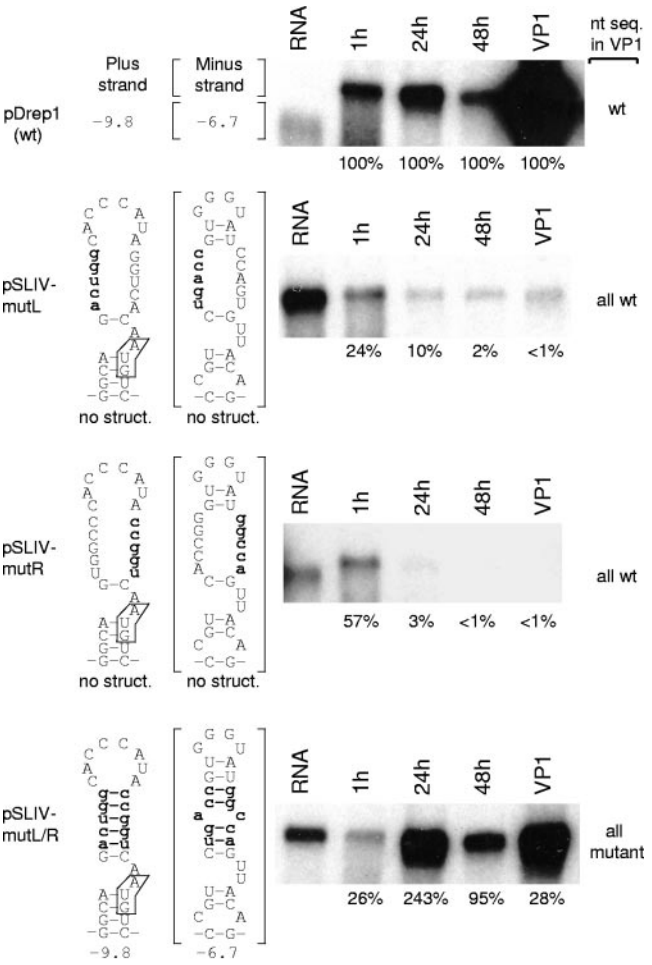

FIG. 3. Integrity of stem IV is required for DI RNA replication as determined by analysis of mutant variants of pDrep1. Mutated bases are shown as lowercase letters, and the calculated free energies of the mutated stem-loops in kcal/mole are indicated. Replication assays were carried out as described in the legend for Fig. 2.

leading to no predicted stem IV structure in either the positive or negative strands (Table 1; Fig. 3). By Northern analysis, 10% or less of wt levels of DI RNA had accumulated by 24 and 48 hpt and less than 1% by 48 hpi in VP1. Sequence analysis of asymmetrically amplified cDNA made from VP1 DI RNA showed the progeny of both mutants to be wt, indicating they had not replicated. By contrast, accumulation of progeny from the double mutant pSLIV-mutL/R in which stem IV had been restored was 243% of wt levels at 24 hpt, 95% at 48 hpt, and 28% in VP1 (Fig. 3). Asymmetrically amplified cDNAs from VP1 (Fig. 3) and VP2 (not shown) DI RNA showed progeny to have retained the double set of mutations. These results, therefore, indicate that the helical region of stem-loop IV either in the positive or negative strand, or both, is required for DI RNA replication. A lower rate of accumulation in the double mutant than in wt at VP1 suggested factors other than the helical nature of the stem, possibly the nucleotide sequence within the stem, might also be important for maximal accumulation.

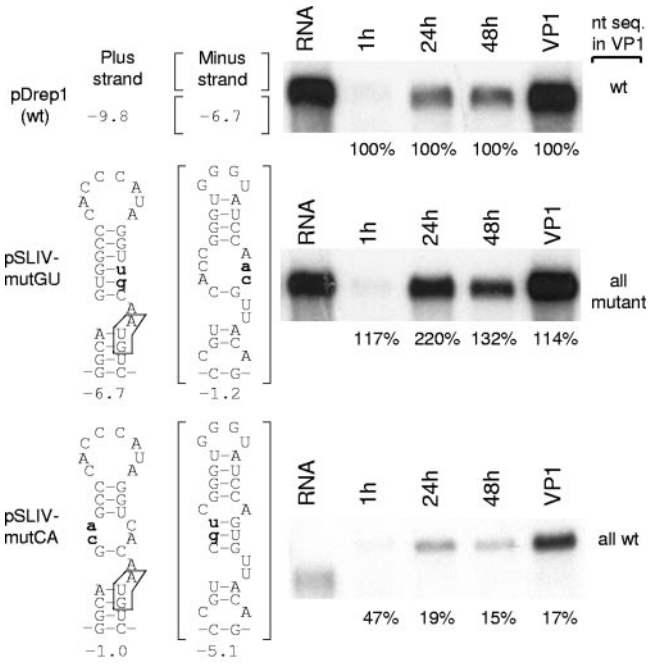

FIG. 4. Integrity of stem IV in the positive strand but not in the negative strand is required for DI RNA replication. Mutated bases are shown, and the calculated free energies of the mutated stem-loops in kcal/mole are indicated. Replication assays were carried out as described for Fig. 2.

Integrity of stem IV in the positive but not the negative strand is required for BCoV DI RNA replication. Base pair covariations among group 2 coronaviruses maintain a stable stem-loop IV in both the positive (free energy range, −12 to −9.8 kcal/mole) and negative (free energy range, −8.9 to −6.7 kcal/mole) strands. The question of which strand of stem-loop IV is required for replication was not answered by the stem IV disruption experiment described above, since the helical region had been disrupted simultaneously in both strands in the two nonreplicating mutants and wt net negative free energy values in both had been restored in the replicating double mutant (Table 1). Therefore, to test the strand requirement for stem-loop IV function, mutations in pDrep1 were made such that only the positive- or negative-strand stem-loop was destabilized, and transcripts were tested for replication. For mutant pSLIV-mutGU, in which stem-loop IV was destabilized in the negative but not the positive strand (Table 1), Northern analysis showed 220% of wt levels at 24 hpt, 132% at 48 hpt, and 114% in VP1, and sequence analysis of asymmetrically amplified cDNAs showed all progeny in VP1 to be mutant sequence, thus indicating transcripts of pSLIV-mutGU had replicated (Fig. 4). By contrast, for mutant pSLIV-mutCA, in which stem-loop IV had been destabilized in the positive but not negative strand, Northern analysis showed an accumulation of 19% of wt levels at 24 hpt, 15% at 48 hpt, and 17% in VP1, and sequence analysis showed all progeny from VP1 to be wt, indicating the mutant had not replicated (Fig. 4). Taken together, these results indicate that the integrity of stem-loop IV for DI RNA replication is required in the positive but not the negative strand and that minor changes in stem sequence at least in the mutated positions do not affect replication.

At least some aspects of wt loop IV sequence are necessary for BCoV DI RNA replication. The phylogenetic conservation of loop IV length and partial primary sequence within group 2 coronaviruses (Fig. 1A) led to the hypothesis that the loop plays a role in the function of stem-loop IV. In the first of two mutants made to test this notion, C3 in the 8-nt loop was deleted, creating pSLIV-mutC198del (Fig. 5A). In the second, C4 and C5 in the loop were changed to Us, creating pSLIV-mut7 (Fig. 5B). The free energies of stem-loop IV in both constructs were identical to wt (Table 1). Although for construct pSLIV-mutC198del only mutant sequences were found in VP1 progeny, thus showing replicability of the mutant molecules, accumulation was twofold less at 24 and 48 hpi and sixfold less in VP1 than wt, indicating wt loop length or sequence integrity may contribute to optimal DI RNA replication. Northern analysis of progeny from pSLIV-mut7, on the other hand, showed accumulation rates of less than 3% of wt throughout, and sequence analyses showed only wt in VP1 progeny, indicating mutant molecules had not replicated. These results taken together indicate that loop IV is an important component of the stem-loop IV *cis*-acting element required for DI RNA replication.

Six cellular proteins, but no detectable viral proteins, bind specifically to wt and functional mutated forms of stem-loop IV RNA. To test the hypothesis that stem-loop IV functions through interactions with viral or cellular proteins, plasmid pSLIV(PB) encoding wt stem-loop IV was linearized at the NcoI site and used to generate uniformly labeled 113-nt transcripts for electrophoretic mobility shift assays. On incubation with lysates of BCoV-infected (Fig. 6, lane 3) or mock-infected (lane 4) cells, three bands of lower mobility became apparent compared to probe incubated with buffer alone (lane 1). When infected cell lysate was treated with proteinase K prior to the addition of probe, no retarded bands were observed (lane 2). These results suggest that all three complexes were formed by interactions with cellular but not viral proteins, although the presence of comigrating complexes with viral proteins could not be ruled out. The complexes, furthermore, were specific to stem-loop IV-containing RNA, since addition of increasing amounts of unlabeled probe as competitor reduced complex formation in a dose-dependent manner (Fig. 6, lanes 5 to 7), whereas the addition of tRNA, a presumed nonspecific competitor, did not (lanes 8 to 10). These results together suggest that stem-loop IV-containing RNA is a binding target for cellular proteins. To determine whether it functions similarly for viral proteins will require further study.

To determine whether the cellular proteins are binding to the 30-nt stem-loop IV element and, simultaneously, to establish whether binding is specific to the wt-like helical structure, electrophoretic mobility shift assays were done in a way that compared the four functional (including wt) and five nonfunctional mutated forms of stem-loop IV. Interestingly, transcripts from all eight mutant constructs were shifted to form three RNA-protein complexes similar to those found with wt stem-loop (Table 1; Fig. 7A to C). These results indicate that at least some cellular proteins are binding to the transcripts regardless of their replicating potential.

To determine the number and sizes of the proteins in the

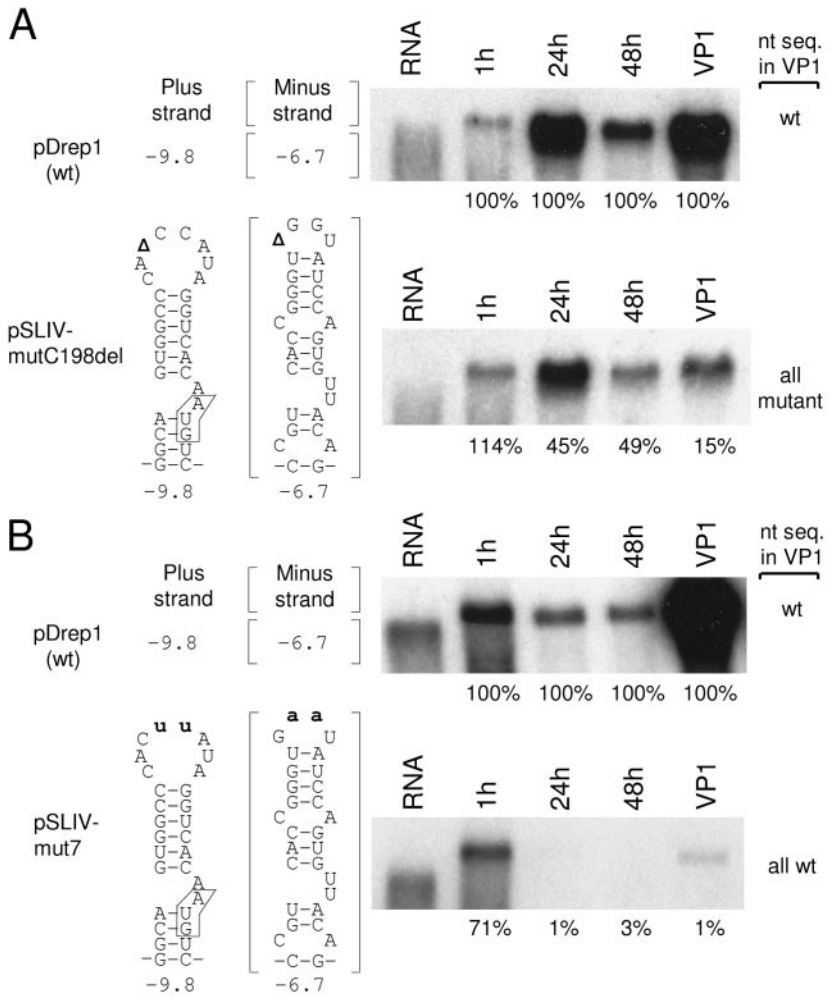

FIG. 5. Wild-type loop IV sequence correlates with maximal DI RNA accumulation. (A) Accumulation and sequence of progeny from DI RNA in which loop IV is shortened from 8 to 7 bases in length (pSLIV-mutC198del). The deleted base is represented by Δ. (B) Accumulation and sequence of progeny from DI RNA in which the loop IV primary sequence is changed (pSLIV-mut7). Assays were carried out as described in the legend for Fig. 2.

complexes, UV cross-linking between the radiolabeled RNA and proteins was done followed by digestion with a mixture of single-strand- and double-strand-specific RNases and SDS-PAGE. By this analysis, nine protein bands representing approximate molecular masses of 25, 26, 28, 33, 39, 41, 45, 48, and 58 kDa were found when wt RNA was used with lysates of uninfected (Fig. 8A, lane 5, and B, lane 8) or infected (Fig. 8A, lanes 1 and 4, and B, lane 9) cells. A potential virus-specific protein band of around 35 kDa, appearing in lane 1 of Fig. 8A and lane 9 of Fig. 8B, was not routinely observed (Fig. 8A, lane 4, and data not shown), suggesting its appearance was artifactual. These results suggested, as did the results of electrophoretic mobility shift experiments, that the proteins binding the stem-loop IV region were cellular. The elimination of all nine bands with proteinase K treatment (Fig. 8A, lane 2, and B, lane 1), furthermore, demonstrated their protein identity. Additionally, all nine cellular proteins bound specifically to the stem-loop IV-containing RNA, since addition of a 1,500-fold excess of unlabeled transcript prevented complex formation (Fig. 8A, lane 3), whereas the same amount of yeast tRNA did not (Fig. 8A, lane 4).

Interestingly, whereas all nine cellular proteins bound probe from wt (Fig. 8A, lanes 1, 4, and 5, and B, lanes 8 and 9) and replicating mutant constructs (mutGU) (Fig. 8A, lane 8, mutL/R and mutC198del, and B, lanes 3 and 4, respectively), only three cellular proteins with molecular masses of 33, 45, and 48 kDa were detectable from lysates of nonreplicating mutants (Fig. 8A, lanes 7 [mutDel] and 9 [mutCA], and B, lanes 5 [mutR], 6 [mutL], and 7 [mut7]). In addition, by comparison with wt and replicating mutants, the amounts of these three protein species were reduced. These data together indicate the six proteins with molecular masses of 25, 26, 28, 39, 41, and 58 kDa, and to a lesser extent those with molecular masses of 33, 45, and 48 kDa, were interacting with stem-loop IV in a higher-order-dependent manner and suggest that the interaction might reflect a mechanistic feature of stem-loop IV function in BCoV DI RNA replication.

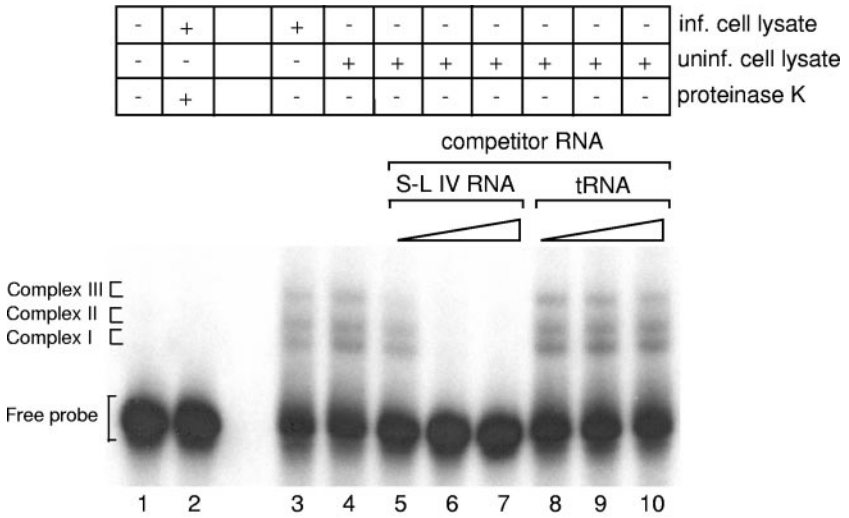

FIG. 6. Cellular proteins bind specifically to stem-loop IV-containing RNA. A uniformly labeled 113-nt stem-loop IV-containing RNA probe was used in electrophoretic mobility shift assays as indicated. Probe treatments: lane 1, incubated with buffer; lane 2, incubated with proteinase K-treated infected cell lysate; lane 3, incubated with infected cell lysate; lane 4, incubated with uninfected cell lysate; lanes 5 to 7, incubated with uninfected cell lysate to which had been added 5, 10, and 15 μg of unlabeled probe RNA, representing a 500-, 1,000-, and 1,500-fold molar excess, respectively; lanes 8 to 10, incubated with uninfected cell lysate to which had been added 5, 10, and 15 μg yeast tRNA, respectively.

DISCUSSION

In this study, we have shown by enzyme structure probing the existence of a predicted bulged stem-loop IV mapping at nt 186 through 215 and therefore lying mostly within the 210-nt 5′ UTR of BCoV DI RNA. Stem-loop IV shows phylogenetic conservation in structure and largely also in sequence among the group 2 coronaviruses and, although it is predicted to exist in the negative strand as well, it was shown by mutation analysis in DI RNA to function in replication only in the positive strand. At least part of the sequence in loop IV was found to be essential for DI RNA replication. Not analyzed for function in our experiments were loop nt 201 to 204 (Fig. 1), which showed some sensitivity to the double-strand-specific nuclease and thus may be at times base-paired with other regions of the genome. Interactions of this kind might be involved in loop IV function. Protein binding studies, furthermore, demonstrated a specific binding of six cellular proteins to wt and mutated forms of stem-loop IV in molecules that replicate, but not to mutated forms in nonreplicating molecules. The binding of cellular proteins, therefore, correlated with both the replicating ability of the DI RNA and a higher-order structure for the stem-loop IV sequence. The binding of viral proteins to wt stem-loop IV was not apparent in gel shift and UV cross-linking experiments, but further studies will be needed to rigorously rule out interaction with viral proteins.

It is not currently known whether the six cellular protein species represent intact (e.g., disulfide-linked) molecules or disassembled polypeptides of larger proteins, nor is the identity of any of the proteins known. Since cell lysis was done in the reducing environment of 1 mM DTT (35), some of the bands may represent subunits of larger disulfide-linked structures. The fact that the conserved loop IV sequence of 5′-CACCCA UA-3′ in group 2 coronaviruses contains the ACCCA motif also found in 5′-ACCCACCC-3′, a PCBP2-binding sequence in the poliovirus genome (27), led us to test whether this 39-kDa protein was one of those binding stem-loop IV. The binding of PCBP2 to other regions of the coronavirus genome has been reported (19, 22). An electrophoretic mobility supershift assay with antiserum to PCBP2 when incubated with cell lysate either before or after the RNA binding reaction, however, demonstrated no supershifted product, indicating PCBP2 probably does not bind stem-loop IV (data not shown). Nor was supershifting observed when antiserum to the 47-kDa La protein, another cellular protein known to react with a variety of cellular and viral RNAs (reference 34 and references therein), was tested in the same way (data not shown). To our knowledge, in no previous study has a protein been identified that binds to the region of the coronavirus genome encompassing stem-loop IV.

Is there a stem-loop IV equivalent in coronavirus groups 1 and 3 and in the SARS coronavirus? Since the coronavirus genomic 5′ UTRs range in length from 210 nt in BCoV to 528 in infectious bronchitis coronavirus (IBV), it is not immediately apparent what predicted folded structures might be homologous among them. By the arbitrary criteria of (i) the most probable higher-order structure as predicted by the Zuker algorithm (i.e., the structures simultaneously showing the lowest free energy and promiscuity [i.e., pnum] values [24, 42]), (ii) distance from the genome 5′ terminus (and hence also from stem-loop III, a predicted homolog found similarly positioned from the 5′ end in groups 1, 2, and 3 [28]), and (iii) apparent conserved features, such as loop sequence, we postulate likely homologs of stem-loop IV in group 1 and the SARS coronavirus but a less likely homolog in group 3 (the free energy values and positions of postulated stem-loop IV structures are noted in Fig. 9). In the group I coronaviruses, a hexaloop sequence in the postulated stem-loop IV is conserved (UU[U/C]CGU) and appears three times (in 229E the second loop is a pentaloop [UUCCG]) on stems that do not closely resemble one another (Fig. 9). Interestingly, in the SARS coronavirus a

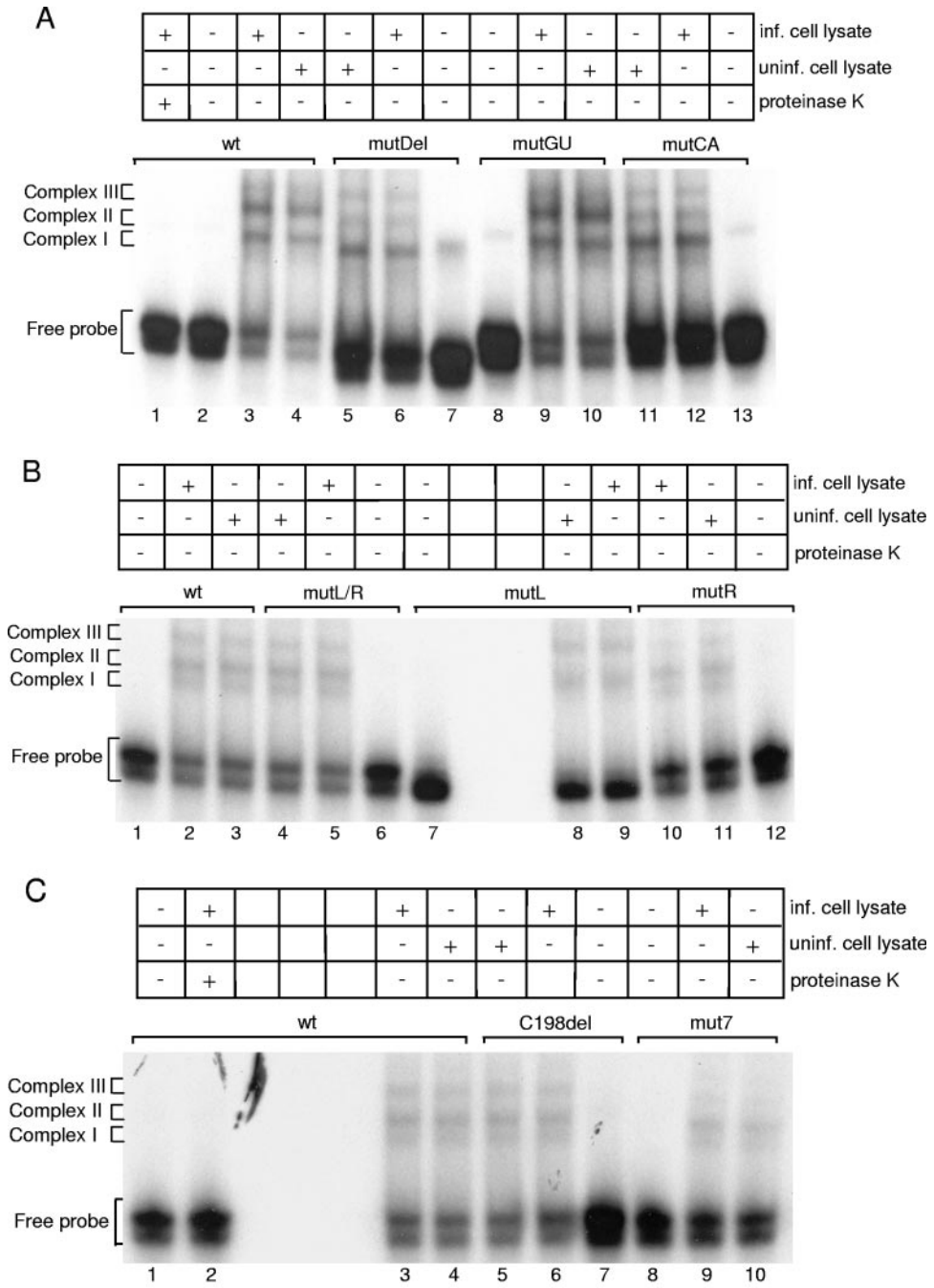

FIG. 7. Cellular proteins bind to both replicating and nonreplicating mutated forms of stem-loop IV RNA. Electrophoretic mobility shift assays were done with radiolabeled transcripts made from the indicated wt and mutant constructs. All probes were 113 nt in length except for the probe from pSLIV-mutDel, which was 93 nt in length. In some cases, two isoforms of the free probe were present. Names of mutants used in the figure are abbreviations.

group I-like stem-loop IV appears twice with a predicted GNRA tetraloop immediately preceding the open reading frame (ORF) 1 start codon. We have used the terms stem-loops IV-1 to IV-3 to identify these stem-loop structures. In light of recent discoveries that the SARS coronavirus has group 2-like properties in its RdRp sequence (32) and in its 3′ UTR structure (15), we find it surprising that a predicted stem-loop IV analog is group 1-like. What ramifications these differences have in postulated coronavirus genomic 5′ and 3′ end interactions (33) remain to be determined.

In IBV, a predicted stable stem-loop with a structure loosely resembling those in group I and SARS coronaviruses is found (Fig. 9). It, however, maps at position 325 rather than between nt 168 and 194 as for stem-loops IV in groups 1 and 2, suggesting that perhaps there is no group 3 stem-loop IV homolog in IBV or that perhaps our second arbitrary criterion for pre-

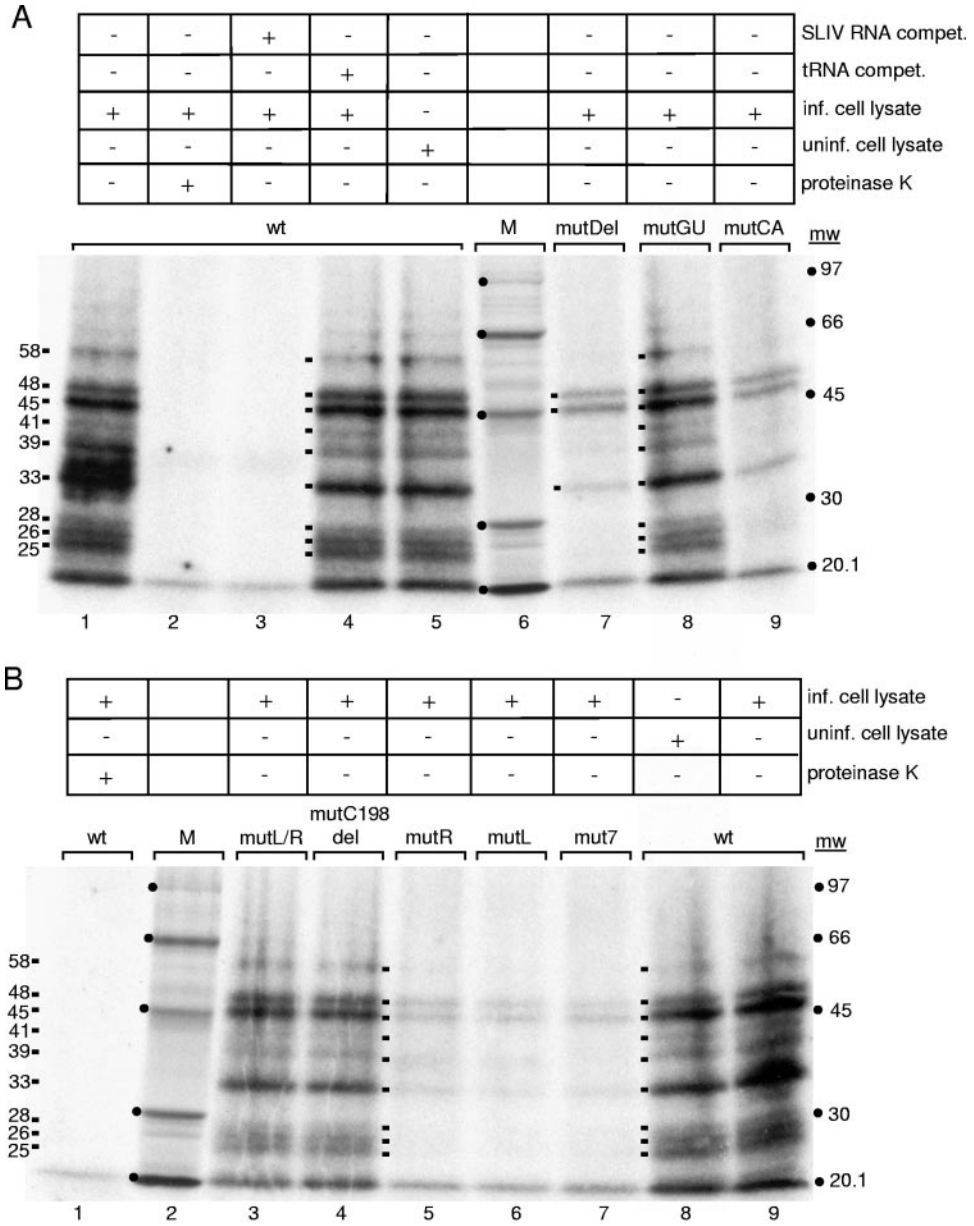

FIG. 8. Nine cellular proteins bind stem-loop IV RNA, but only six bind specifically. UV cross-linking was done on protein binding reaction mixtures prepared as described in the legend for Fig. 7. Reaction products were then digested simultaneously with RNases T_1, A, and CV1, as described in the text, and electrophoretically separated on 10% SDS-PAGE gels. Where indicated, 15 μg (1,500-fold molar excess) of competitor RNA was incubated with the cell lysate prior to the addition of the radiolabeled probe. Numbers to the right indicate molecular weight positions as determined by molecular weight markers, and those to the left indicate estimated molecular weights of the radiolabeled proteins.

dicting homologous stem-loop IV structures is not applicable in the case of such a long 5′ UTR.

How does stem-loop IV in BCoV DI RNA function mechanistically in replication? Previous studies using BCoV DI RNA had indicated that ORF 1a is translated by ribosomal scanning from the 5′ end of the genome and, thus, it is unlikely that stem-loop IV is a required structure for directing an internal entry of ribosomes for the translation of ORF 1a (31). We therefore propose that stem-loop IV along with stem-loop III functions in the formation of the RNA replication complex. This concept is consistent with the observation that stem-loop IV is part of a contiguous 421-nt sequence found in the BCoV DI RNA but missing in subgenomic mRNA 7 that, despite being identical to the DI RNA replicon in every other aspect, fails to replicate after transfection into helper virus-infected cells (7). Since the higher-order integrity of stem IV in only the positive RNA strand is required for replication (Table 1; Fig. 4), one possibility is that it functions as a *cis*-acting element in the initiation of negative-strand synthesis. Such a function for 5′-proximal structures has been demonstrated in other plus-strand RNA viruses where physical interactions between the genome 5′ and 3′ ends are necessary for genome replication (4,

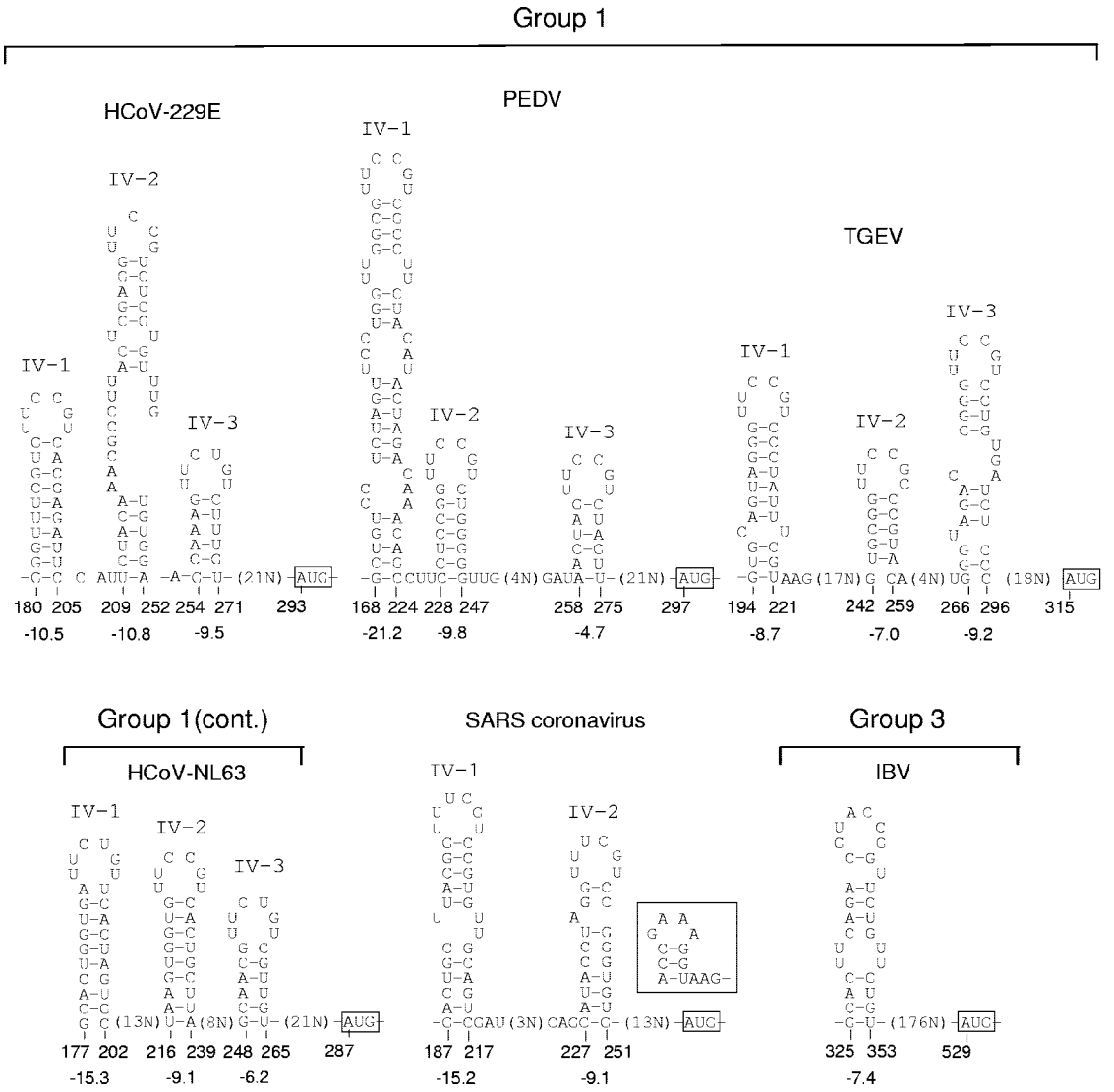

FIG. 9. Potential stem-loop IV homologs in coronavirus groups 1 and 3 and the SARS-CoV. Potential stem-loop IV homologs with accompanying calculated free energy values in kcal/mol for the group 1 coronaviruses, including the recently described HCoV-NL63, and the group 3 coronaviruses, as predicted by the Zuker *mfold* algorithm, are depicted. Note the similarities in predicted loop structures of the group 1 coronaviruses and SARS-CoV. In SARS-CoV, a GNRA tetraloop (shown in inset) is predicted at a site just upstream of the ORF 1 start codon.

11, 13, 17, 25, 29, 34, 37). In BCoV DI RNA the interaction of stem-loop III with viral N and cellular proteins and stem-loop IV with cellular proteins (data shown here and unpublished data) would suggest that bridging and circularization, if it occurs, would be through proteins as previously postulated (33). It is also quite possible that since N binds to the leader motif UCUAAAC (26), which in BCoV is found in stem-loop II (7), and is required for genome replication (1, 30) that protein interactions involving stem-loops II, III, and IV together function in replication complex formation.

A positive correlation between the binding of six cellular proteins to stem-loop IV and replicating ability of the DI RNA suggests that stem-loop IV functions in replication through its interaction with these proteins. Further analyses to identify the proteins and determine how they interact with each other and with stem-loop IV should provide insight into how stem-loop IV functions in DI RNA replication.

ACKNOWLEDGMENTS

We thank Cary Brown, Kimberley Nixon, Aykut Ozdarendeli, Gwyn Williams, and Hung-Yi Wu for valuable discussions.

This work was supported by grant AI14267 from the National Institute of Allergy and Infectious Diseases, grant 92-37204-8046 from the U.S. Department of Agriculture, and by funds from the University of Tennessee, College of Veterinary Medicine, Center of Excellence Program for Livestock Diseases and Human Health.

REFERENCES

1. **Almazan, F., C. Galan, and L. Enjuanes.** 2004. The nucleoprotein is required for efficient coronavirus genome replication. J. Virol. **78:**12683–12688.
2. **Andino, R., G. E. Rieckhof, P. L. Achacoso, and D. Baltimore.** 1993. Poliovirus RNA synthesis utilizes an RNP complex formed around the 5′-end of viral RNA. EMBO J. **12:**3587–3598.

3. **Andino, R., G. E. Rieckhof, and D. Baltimore.** 1990. A functional ribonucleoprotein complex forms around the 5′ end of poliovirus RNA. Cell **63:**369–380.
4. **Barton, D. J., B. J. O'Donnell, and J. B. Flanegan.** 2001. 5′ cloverleaf in poliovirus RNA is a cis-acting replication element required for negative-strand synthesis. EMBO J **20:**1439–1448.
5. **Bedard, K. M., B. L. Walter, and B. L. Semler.** 2004. Multimerization of poly(rC) binding protein 2 is required for translation initiation mediated by a viral IRES. RNA **10:**1266–1276.
6. **Blyn, L. B., J. S. Towner, B. L. Semler, and E. Ehrenfeld.** 1997. Requirement of poly(rC) binding protein 2 for translation of poliovirus RNA. J. Virol. **71:**6243–6246.
7. **Chang, R. Y., M. A. Hofmann, P. B. Sethna, and D. A. Brian.** 1994. A *cis*-acting function for the coronavirus leader in defective interfering RNA replication. J. Virol. **68:**8223–8231.
8. **Chang, R. Y., R. Krishnan, and D. A. Brian.** 1996. The UCUAAAC promoter motif is not required for high-frequency leader recombination in bovine coronavirus defective interfering RNA. J. Virol. **70:**2720–2729.
9. **Chen, J., A. Noueiry, and P. Ahlquist.** 2001. Brome mosaic virus protein 1a recruits viral RNA2 to RNA replication through a 5′-proximal RNA2 signal. J. Virol. **75:**3207–3219.
10. **Fabian, M. R., and K. A. White.** 2004. 5′-3′ RNA-RNA interaction facilitates cap- and poly(A) tail-independent translation of tomato bushy stunt virus mRNA: a potential common mechanism for tombusviridae. J. Biol. Chem. **279:**28862–28872.
11. **Frolov, I., R. Hardy, and C. M. Rice.** 2001. *cis*-acting RNA elements at the 5′ end of Sindbis virus genome RNA regulate minus- and plus-strand RNA synthesis. RNA **7:**1638–1651.
12. **Gamarnik, A. V., and R. Andino.** 2000. Interactions of viral protein 3CD and poly(rC) binding protein with the 5′ untranslated region of the poliovirus genome. J. Virol. **74:**2219–2226.
13. **Gamarnik, A. V., and R. Andino.** 1998. Switch from translation to RNA replication in a positive-stranded RNA virus. Genes Dev. **12:**2293–2304.
14. **Gamarnik, A. V., and R. Andino.** 1997. Two functional complexes formed by KH domain containing proteins with the 5′ noncoding region of poliovirus RNA. RNA **3:**882–892.
15. **Goebel, S. J., J. Taylor, and P. S. Masters.** 2004. The 3′ *cis*-acting genomic replication element of the severe acute respiratory syndrome coronavirus can function in the murine coronavirus genome. J. Virol. **78:**7846–7851.
16. **Guo, L., E. M. Allen, and W. A. Miller.** 2001. Base-pairing between untranslated regions facilitates translation of uncapped, nonpolyadenylated viral RNA. Mol. Cell **7:**1103–1109.
17. **Herold, J., and R. Andino.** 2001. Poliovirus RNA replication requires genome circularization through a protein-protein bridge. Mol. Cell **7:**581–591.
18. **Hofmann, M. A., R. Y. Chang, S. Ku, and D. A. Brian.** 1993. Leader-mRNA junction sequences are unique for each subgenomic mRNA species in the bovine coronavirus and remain so throughout persistent infection. Virology **196:**163–171.
19. **Huang, P., and M. M. Lai.** 1999. Polypyrimidine tract-binding protein binds to the complementary strand of the mouse hepatitis virus 3′ untranslated region, thereby altering RNA conformation. J. Virol. **73:**9110–9116.
20. **Khromykh, A. A., H. Meka, K. J. Guyatt, and E. G. Westaway.** 2001. Essential role of cyclization sequences in flavivirus RNA replication. J. Virol. **75:**6719–6728.
21. **Kim, K. H., and C. L. Hemenway.** 1999. Long-distance RNA-RNA interactions and conserved sequence elements affect potato virus X plus-strand RNA accumulation. RNA **5:**636–645.
22. **Li, H. P., P. Huang, S. Park, and M. M. Lai.** 1999. Polypyrimidine tract-binding protein binds to the leader RNA of mouse hepatitis virus and serves as a regulator of viral transcription. J. Virol. **73:**772–777.
23. **Makino, S., and M. M. Lai.** 1989. High-frequency leader sequence switching during coronavirus defective interfering RNA replication. J. Virol. **63:**5285–5292.
24. **Mathews, D. H., J. Sabina, M. Zuker, and D. H. Turner.** 1999. Expanded sequence dependence of thermodynamic parameters improves prediction of RNA secondary structure. J. Mol. Biol. **288:**911–940.
25. **Miller, E. D., C. A. Plante, K. H. Kim, J. W. Brown, and C. Hemenway.** 1998. Stem-loop structure in the 5′ region of potato virus X genome required for plus-strand RNA accumulation. J. Mol. Biol. **284:**591–608.
26. **Nelson, G. W., S. A. Stohlman, and S. M. Tahara.** 2000. High affinity interaction between nucleocapsid protein and leader/intergenic sequence of mouse hepatitis virus RNA. J. Gen. Virol. **81:**181–188.
27. **Parsley, T. B., J. S. Towner, L. B. Blyn, E. Ehrenfeld, and B. L. Semler.** 1997. Poly(rC) binding protein 2 forms a ternary complex with the 5′-terminal sequences of poliovirus RNA and the viral 3CD proteinase. RNA **3:**1124–1134.
28. **Raman, S., P. Bouma, G. D. Williams, and D. A. Brian.** 2003. Stem-loop III in the 5′ untranslated region is a *cis*-acting element in bovine coronavirus defective interfering RNA replication. J. Virol. **77:**6720–6730.
29. **Ray, D., H. Na, and K. A. White.** 2004. Structural properties of a multifunctional T-shaped RNA domain that mediate efficient tomato bushy stunt virus RNA replication. J. Virol. **78:**10490–10500.
30. **Schelle, B., N. Karl, B. Ludewig, S. G. Siddell, and V. Thiel.** 2005. Selective replication of coronavirus genomes that express nucleocapsid protein. J. Virol. **79:**6620–6630.
31. **Senanayake, S. D., and D. A. Brian.** 1999. Translation from the 5′ untranslated region (UTR) of mRNA 1 is repressed, but that from the 5′ UTR of mRNA 7 is stimulated in coronavirus-infected cells. J. Virol. **73:**8003–8009.
32. **Snijder, E. J., P. J. Bredenbeek, J. C. Dobbe, V. Thiel, J. Ziebuhr, L. L. Poon, Y. Guan, M. Rozanov, W. J. Spaan, and A. E. Gorbalenya.** 2003. Unique and conserved features of genome and proteome of SARS-coronavirus, an early split-off from the coronavirus group 2 lineage. J. Mol. Biol. **331:**991–1004.
33. **Spagnolo, J. F., and B. G. Hogue.** 2000. Host protein interactions with the 3′ end of bovine coronavirus RNA and the requirement of the poly(A) tail for coronavirus defective genome replication. J. Virol. **74:**5053–5065.
34. **Teterina, N. L., D. Egger, K. Bienz, D. M. Brown, B. L. Semler, and E. Ehrenfeld.** 2001. Requirements for assembly of poliovirus replication complexes and negative-strand RNA synthesis. J. Virol. **75:**3841–3850.
35. **Thomson, A. M., J. T. Rogers, C. E. Walker, J. M. Staton, and P. J. Leedman.** 1999. Optimized RNA gel-shift and UV cross-linking assays for characterization of cytoplasmic RNA-protein interactions. BioTechniques **27:**1032–1042.
36. **Van Den Born, E., A. P. Gultyaev, and E. J. Snijder.** 2004. Secondary structure and function of the 5′-proximal region of the equine arteritis virus RNA genome. RNA **10:**424–437.
37. **Vlot, A. C., and J. F. Bol.** 2003. The 5′ untranslated region of alfalfa mosaic virus RNA 1 is involved in negative-strand RNA synthesis. J. Virol. **77:**11284–11289.
38. **Walter, B. L., T. B. Parsley, E. Ehrenfeld, and B. L. Semler.** 2002. Distinct poly(rC) binding protein KH domain determinants for poliovirus translation initiation and viral RNA replication. J. Virol. **76:**12008–12022.
39. **Woo, P. C., S. K. Lau, C. M. Chu, K. H. Chan, H. W. Tsoi, Y. Huang, B. H. Wong, R. W. Poon, J. J. Cai, W. K. Luk, L. L. Poon, S. S. Wong, Y. Guan, J. S. Peiris, and K. Y. Yuen.** 2005. Characterization and complete genome sequence of a novel coronavirus, coronavirus HKU1, from patients with pneumonia. J. Virol. **79:**884–895.
40. **Wu, H. Y., J. S. Guy, D. Yoo, R. Vlasak, E. Urbach, and D. A. Brian.** 2003. Common RNA replication signals exist among group 2 coronaviruses: evidence for in vivo recombination between animal and human coronavirus molecules. Virology **315:**174–183.
41. **You, S., B. Falgout, L. Markoff, and R. Padmanabhan.** 2001. In vitro RNA synthesis from exogenous dengue viral RNA templates requires long range interactions between 5′- and 3′-terminal regions that influence RNA structure. J. Biol. Chem. **276:**15581–15591.
42. **Zuker, M.** 2003. Mfold web server for nucleic acid folding and hybridization prediction. Nucleic Acids Res. **31:**3406–3415.